EARTH SCIENCES
RESEARCH JOURNAL
Earth Sci. Res. J. Vol. 29, No. 3 (September, 2025): 347 - 362

UNIVERSIDAD NACIONAL DE COLOMBIA

SEISMOLOGY

Characterization of nonlinear dynamic soil properties for seismic site response in Islamabad, Pakistan

Waqas Ahmed[1], Muhammad Waseem[2], Hammad Raza[3], Muhammad Yasir[1], Muhammad Zeeshan[1], Saif Ullah[1], Ihtisham Islam[4]*, Salman Ahmed Khattak[5,6]*

1. National Centre of Excellence in Geology, University of Peshawar, 25120, Peshawar Pakistan.
2. Department of Civil Engineering, University of Engineering and Technology, Peshawar, 25120, Peshawar Pakistan.
3. University of Engineering and Technology, Taxila, 47080, Pakistan.
4. Department of Geology, Shaheed Benazir Bhutto University Sheringal, 18030, Dir Upper Pakistan.
5. State Key Laboratory of Critical Mineral Research and Exploration, Institute of Geochemistry, Chinese Academy of Sciences, Guiyang 550081, China.
6. University of Chinese Academy of Sciences, Beijing 100049, China
*Corresponding authors: ihtisham.islam@sbbu.edu.pk; salman@mail.gyig.ac.cn

ABSTRACT

This study presents a detailed experimental characterization of the small-strain dynamic behavior of fine-grained soils in the Islamabad capital territory, Pakistan, an area of moderate to high seismic hazard with limited site-specific geotechnical data. A comprehensive series of resonant column tests was conducted on reconstituted silty clay and clayey silt samples collected from 15 boreholes across the region. Tests were performed under confining pressures of 50, 100, and 150 kPa to evaluate shear wave velocity, maximum shear modulus (G_{max}), the modulus reduction (G/G_{max}) with shear strain, and strain-dependent damping behavior. Results reveal that Islamabad soils are characteristically stiff at small strains, with G_{max} ranging from approximately 40–80 MPa and increasing systematically with confining pressure, while typical Vs values ranged from 160–260 m/s. The normalize shear modulus (G/G_{max}) curves showed moderate nonlinearity, with G/G_{max} reducing to 0.3–0.5 at maximum strain levels (~0.1–0.2%). Reference strain (γ_{ref}) values obtained from curve fitting fell between ~0.02–0.08%, further quantifying the onset of modulus reduction. Damping ratios increased from ~0.5% at microstrains to a maximum of 8–12% at higher strains, with minor variation across confining pressures. When compared with standard empirical models, the measured curves exhibited stiffer behavior and lower damping at equivalent strains, highlighting the importance of site-specific calibration. These findings provide critical input for improving seismic site response analyses in Islamabad, directly informing local microzonation studies and contributing to the refinement of Pakistan's seismic design guidelines.

Keywords: Malatya, Eastern Anatolia Fault zone, earthquake, GNSS, seismicity, deformation.

Caracterización de las propiedades dinámicas no lineales del suelo para la respuesta sísmica en Islamabad, Pakistán

RESUMEN

Este estudio presenta una caracterización experimental detallada del comportamiento dinámico de pequeña deformación en los suelos de grano fino del territorio de Islamabad, Pakistan, una área de riesgo sísmico de moderado a alto con limitada información geotécnica específica. Para ello se realizó una amplia serie de pruebas de columna resonante en muestras de arcilla limosa y limo arcilloso recolectadas en 15 perforaciones a lo largo de la región. Las pruebas se realizaron bajo presión de compresión de 50, 100 y 150 KPa para evaluar la velocidad de la onda transversal (Vs), módulo de corte máximo (G_{max}), el módulo de reducción (G/G_{max}) con corte máximo y comportamiento de amortiguamiento dependiente de la deformación. Los resultados muestran que los suelos de Islamabad son característicamente rígidos con pequeñas deformaciones, con un G_{max} que oscila entre aproximadamente 40 y 80 MPa y aumenta sistemáticamente con la presión de confinamiento, mientras que los valores típicos de Vs oscilaron entre 160 y 260 m/s. Las curvas de módulo de corte normalizado (G/G_{max}) mostraron una no linealidad moderada, con un G/G_{max} reduciéndose a 0,3-0,5 a niveles máximos de deformación (~0,1-0,2%). Los valores de deformación de referencia (γ_{ref}) obtenidos del ajuste de la curva se situaron entre ~0,02 y 0,08%, lo que cuantifica aún más el inicio de la reducción del módulo. Los coeficientes de amortiguamiento aumentaron de ~0,5% a microdeformaciones hasta un máximo de 8-12% a deformaciones más altas, con una variación mínima a través de las presiones de confinamiento. En comparación con los modelos empíricos estándar, las curvas medidas mostraron un comportamiento más rígido y un menor amortiguamiento a deformaciones equivalentes, lo que resalta la importancia de la calibración específica del sitio. Estos hallazgos proporcionan información crucial para mejorar los análisis de respuesta sísmica del sitio en Islamabad, informando directamente los estudios de microzonificación local y contribuyendo al perfeccionamiento de las directrices de diseño sísmico de Pakistán.

Palabras clave: Malatya; zona de fallas del Este de Anatolia; terremoto; GNSS; seismicidad; deformación.

Record
Manuscript received: 12/06/2025
Accepted for publication: 12/09/2025

How to cite this item:
Ahmed, W., Waseem, M., Raza, H., Yasir, M., Zeeshan, M., Ullah, S. Islam, I., & Khattak, S. A. (2025). Characterization of nonlinear dynamic soil properties for seismic site response in Islamabad, Pakistan. *Earth Sciences Research Journal, 29*(3), 347-362. https://doi.org/10.15446/esrj.v29n3.120899

1. Introduction

The Islamabad capital territory (ICT) lies at the tectonic junction of the Indian and Eurasian plates, where active collision processes in the Himalayan front generate significant seismic hazard. This region is seismically classified as zone 2B under the building code of Pakistan (BCP, 2021), corresponding to a peak ground acceleration (PGA) of approximately 0.19–0.26 g for design-level events (BCP, 2021). The proximity of Islamabad to major active faults such as the Main Boundary Thrust and the Hazara-Kashmir Syntaxis increases the likelihood of moderate to strong ground shaking during future earthquakes (Jadoon et al., 2015; Khan et al., 2021). The 2005 Mw 7.6 Kashmir earthquake, which caused over 85,000 fatalities, had an epicenter approximately 100 km from Islamabad and produced significant shaking across the city. Structural damage, including the collapse of the Margalla towers, exposed critical deficiencies in the local understanding of soil behavior under seismic loading (Mahmood et al., 2016).

Despite this high seismic risk, there remains a lack of site-specific geotechnical data to inform seismic hazard assessments in the region. This gap is particularly acute with respect to the small-strain dynamic properties of soils, such as shear modulus and damping ratio, which play a pivotal role in seismic site response. These parameters control wave propagation characteristics, influence spectral amplification, and govern the interaction between soil and structures under dynamic loading (Zhang et al., 2005; Wang and Stokoe, 2022). Without reliable measurements of these properties, engineers are often forced to adopt empirical estimates based on generic soil classifications or indirect correlations approaches that introduce uncertainty into seismic design and ground motion modeling (Boore et al., 2011; Adeel et al., 2023).

Globally, small-strain soil behavior has been widely characterized through standardized empirical models, including those developed by Seed and Idriss (1970), Vucetic and Dobry (1991), and Darendeli (2001). These frameworks provide modulus reduction (G/G_{max}) and damping ratio (D) curves as functions of cyclic shear strain, typically parameterized by factors such as plasticity index, confining pressure, and over consolidation ratio. Because of their broad acceptance, these models are embedded in most modern site response software packages, such as DEEPSOIL and STRATA, and continue to play a central role in engineering practice.

However, these models were primarily developed from soils in different geological settings, often focusing on granular sands or high-plasticity clays from the United States and Japan. Applying them uncritically to Islamabad, with its unique depositional history and fine-grained, low- to intermediate-plasticity alluvium, risks introducing bias into seismic hazard analysis. Such mismatches can lead to erroneous predictions of ground motion amplification and structural demand, as highlighted by prior studies (Guerreiro et al., 2012; Vardanega and Bolton, 2013). This underscores the need for laboratory-based characterization of Islamabad soils to establish reliable local modulus reduction and damping curves.

In Pakistan, and particularly in Islamabad, limited studies have reported in-situ or laboratory-based dynamic properties of soils. Site classification is typically inferred from surface geology, standard penetration test (SPT) blow counts, or proxy-based Vs30 correlations, without validation from resonant column or cyclic triaxial testing (Khan and Khan, 2016; Aaqib et al., 2024). Previous investigations by Khan et al. (2021) and Adeel et al. (2023) attempted to map Vs30 across the Islamabad–Rawalpindi region using empirical correlations, but these estimates remain unverified due to the absence of measured shear wave velocities and modulus reduction curves for local soils. Recent microzonation efforts have also highlighted this data gap, calling for the acquisition of site-specific dynamic soil properties to support more robust seismic hazard models (Khan and Khan, 2017; Raza et al., 2025).

Among the laboratory methods available for evaluating the small-strain stiffness and damping behavior of soils, the resonant column test remains one of the most effective and widely accepted approaches. Resonant column testing offers a controlled environment for evaluating shear wave velocity (Vs), shear modulus (G), and damping ratio over strain levels typically ranging from 10^{-4}% to 10^{-2}%, which corresponds to the range experienced during moderate earthquakes in near-surface soils (Hardin and Drnevich, 1972; Cha et al., 2014). Furthermore, the ability to vary confining pressure allows simulation of in-situ stress conditions across different soil depths, enhancing the representativeness of the results for site response applications. Dry-state resonant column testing is particularly suitable for low-plasticity fine-grained soils, where small-strain behavior is not significantly influenced by pore water pressure (Blaker and DeGroot, 2020; Mog and Anbazhagan, 2022).

Islamabad's near-surface geology consists predominantly of Quaternary alluvial and colluvial deposits, including silty clays, clayey silts, and occasional sandy layers overlying weathered bedrock (Sheikh et al., 2008; Khan and Khan, 2016). These fine-grained soils often exhibit low to moderate plasticity, relatively stiff consistency, and complex microstructure due to mixed depositional and diagenetic processes. As such, they are unlikely to conform to standard empirical modulus reduction models developed for either high-plasticity clays or granular soils. Understanding the actual nonlinear stress-strain response of these materials under cyclic loading is essential for realistic site response predictions and the development of locally calibrated design spectra.

To date, no laboratory-based modulus reduction (G/G_{max}) or damping ratio (D) curves have been reported for Islamabad soils. Existing site response studies have relied on generic empirical models or indirect correlations, which introduces significant uncertainty into seismic hazard evaluations. This absence of laboratory-derived curves represents a critical research gap that limits reliable microzonation and seismic design in the region. To address this critical knowledge gap, the present study undertakes a comprehensive laboratory investigation of the small-strain dynamic properties of silty clay and clayey silt soils in the Islamabad region. Reconstituted specimens from 15 representative borehole locations were tested in a resonant column apparatus under isotropic confining pressures of 50 kPa, 100 kPa, and 150 kPa. These pressure levels were selected to simulate shallow to intermediate depths typically relevant for seismic site classification and response modelling. The study focuses on: (1) to measure shear wave velocity (Vs) and maximum shear modulus (G_{max}) of Islamabad soils under varying confining pressures; (2) to characterize the modulus reduction (G/G_{max}) and damping ratio (D) behaviour across a representative strain range; and (3) to evaluate the applicability of standard empirical models (e.g., Darendeli, and Vucetic & Dobry) for predicting the nonlinear behaviour of these soils.

The results provide the first high-resolution laboratory dataset of G/G_{max} and D–γ curves for Islamabad's native fine-grained soils and offer insight into how these materials respond under cyclic loading conditions. By comparing the measured behavior against well-established models, the study also assesses the extent to which existing empirical frameworks are suitable for use in this region. Ultimately, the findings support the development of improved input parameters for seismic site response analyses and contribute to a more reliable foundation for performance-based earthquake engineering and seismic code development in Pakistan.

2. Materials and Methods

2.1 Site and Soil Sampling

Soil samples were collected from multiple sites within the Islamabad capital territory, covering a range of typical local soil conditions (Fig. 1). The area's geology consists of Quaternary alluvial deposits (valley-fill silts, clays, and sands) overlying denser Pleistocene sediments and weathered rock (limestone) toward the Margalla Hills. These Quaternary deposits, composed primarily of low-plasticity silts and clays, play a critical role in seismic response, as their stiffness and damping properties control the amplification of ground motions within the city. This study therefore focused on fine-grained soils that are common in the top 20 m across the city.

Undisturbed samples were obtained using thin-walled Shelby tubes, which were pushed in boreholes at depths of 5–15 m. In total, 25 tube samples were collected from 15 locations. Each sample was immediately sealed and transported to the laboratory for testing. The borehole sites were strategically selected to represent the major geomorphological units of Islamabad, including alluvial plains, colluvial deposits, and transitional zones near the Margalla Hills. This ensured coverage of the dominant fine-grained soils (silty clays and clayey silts) that govern seismic response. Sites were also distributed across areas of ongoing urban development and seismic microzonation interest, so that the dataset would be both scientifically representative and practically relevant for hazard assessment.

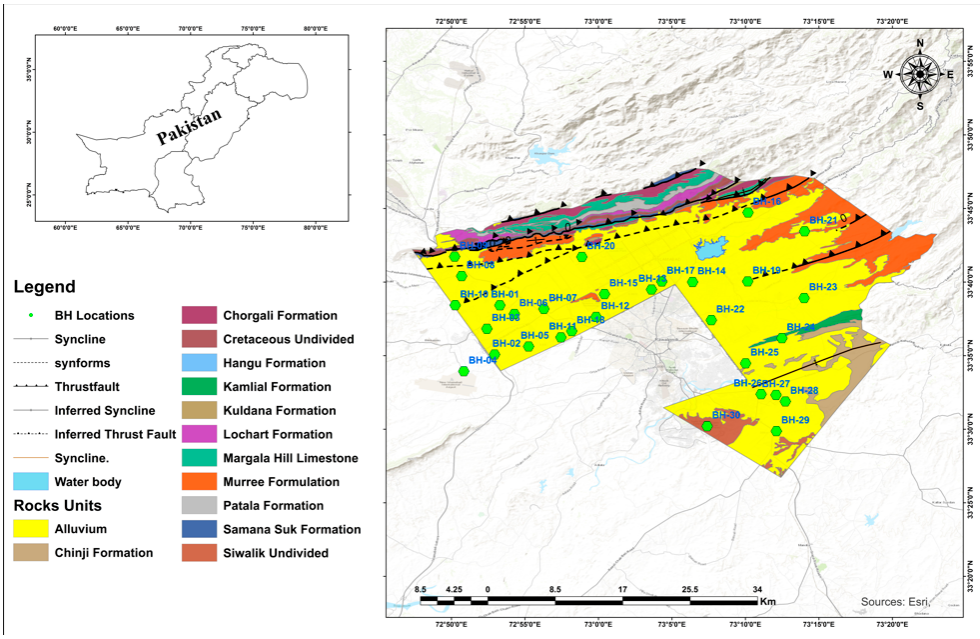

Figure 1. Geological map of Islamabad showing borehole (BH) locations and major rock formations. Structural features such as thrust faults and synclines are also depicted for regional context

2.2 Resonant Column (RC) Testing

Accurate evaluation of dynamic soil properties requires careful specimen preparation, particularly in resonant column (RC) testing. In this study, tests were performed on reconstituted specimens of silty clay with a plasticity index (PI) < 9, indicative of low-plasticity, silt-dominated behavior. Although reconstitution may alter natural soil fabric and cementation, previous studies have shown that for low-plasticity silts and silty clays, the small-strain stiffness and damping behavior of intact and reconstituted specimens are broadly comparable (Blaker & DeGroot, 2020; Mog & Anbazhagan, 2022).

Specimens were tested in the dry state, consistent with the current configuration of the GCTS resonant column apparatus (Fig. 2), which does not support back-pressure saturation or pore water pressure measurements. Dry testing is commonly used in similar studies and is considered reliable for small-strain behavior in low-plasticity soils. Blaker and DeGroot (2020) compared dry and saturated tests on low-plasticity silty clays and found that the shear modulus and damping ratios at small strains ($\gamma < 0.001\%$) were essentially unchanged by saturation. Mog and Anbazhagan (2022) also demonstrated that for silty clays, dry-state testing captured the small-strain stiffness plateau reliably, noting only minor differences in damping ratio at larger strains (>0.1%) due to the absence of pore pressure effects. Similarly, Bozyigit and Altun (2023) reported negligible differences in small-strain stiffness for dry and saturated tests on silty sand–clay mixtures, supporting the appropriateness of dry-state testing in resonant column studies of low-PI soils. For small-strain behavior where interparticle water movement is minimal dry testing provides representative and reliable dynamic properties for engineering applications.

All tested specimens were prepared by reconstituting air-dried soil from each sampling location. The soil was oven-dried at 105 °C, gently pulverized, and sieved through a No. 40 mesh to remove oversized particles. The reconstituted material was statically compacted in five uniform layers inside a cylindrical mold. This procedure achieved target dry densities of 1.65–1.80 g/cm³, which approximate the in-situ conditions observed in borehole logs and confirmed by laboratory moisture–density relationships. Each specimen was trimmed to a standard size (height: 100 mm, diameter: 50 mm), encased in a latex membrane, and mounted in the resonant column cell between beryllium copper end caps. A vacuum of approximately 20 kPa was applied to ensure membrane conformity and eliminate air voids between the sample and confining chamber. The top platen was connected to the drive system and displacement transducers, while the bottom platen remained fixed. Isotropic confining pressures of 50, 100, and 150 kPa were applied using compressed air, representing stress levels typical of depths up to 10–15 m in Islamabad soils. Before each stage, the specimen was reconsolidated under the new confining pressure and allowed to equilibrate for at least 30 minutes, ensuring stable conditions and eliminating residual strain effects from prior loading. This procedure minimized the risk of bias in stiffness and damping measurements across different stress level.

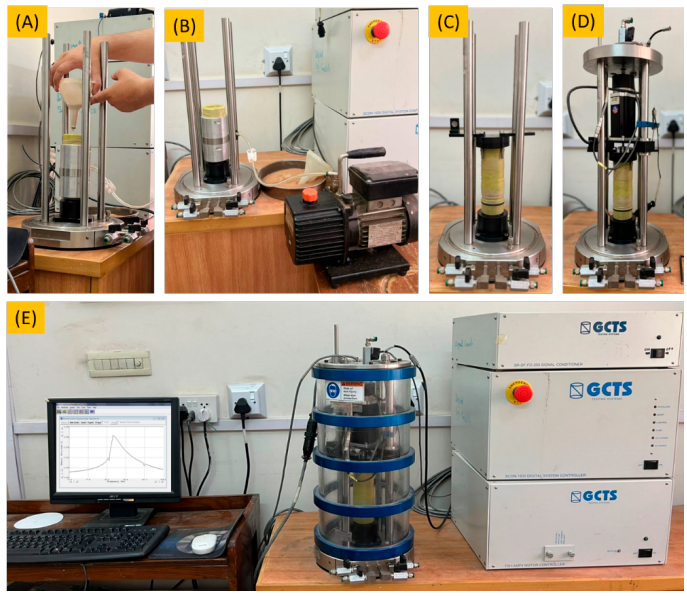

Figure 2. (A–D) Setup and operation of the GCTS resonant column test system for soil samples, including sample preparation, cell assembly, and testing phases; (E) Complete resonant column test system

The sample was excited at low torsional amplitudes to induce shear strains of ~0.0001%–0.001%. The system swept across excitation frequencies

(typically 50–150 Hz) to identify the fundamental mode. Shear wave velocity (V_s) was calculated using:

$$V_S = (2\pi f_r) \cdot \left(\frac{\eta}{H}\right)$$

and the maximum shear modulus (G_{max}) was obtained from:

$$G_{max} = \rho \cdot V_s^2$$

where ρ is the specimen's mass density, H is specimen height, and η = 0.75 is the mode shape factor.

Drive voltages were progressively increased to generate strain levels up to ~0.2%. At each strain level, the updated resonant frequency and free vibration decay were measured. Damping was evaluated using the free vibration decay (FVD) (logarithmic decrement) method:

$$\delta = \ln\left(\frac{A_1}{A_2}\right)$$

$$D = \sqrt{\frac{\delta^2}{4\pi^2 + \delta^2}}$$

where:

A_1 and A_2 are successive peak amplitudes of FVD.

For validation, the half-power bandwidth method was also applied under steady-state vibration (SSV) conditions, consistent with ASTM D4015 procedures:

$$D = \frac{f_2 - f_1}{2f_r}$$

where:

- f_1 and f_2 are the half-power frequencies, and
- f_r is the resonant frequency.

Both methods yielded consistent results in the small-strain range. For nonlinear behavior at higher strains (>0.01%), the FVD method provided more stable and representative damping values due to the inherent asymmetry of frequency response in soil.

Determination of dynamic soil properties in the GCTS resonant column apparatus requires precise calibration of the drive mechanism to account for its mass moment of inertia (I_o). This calibration was conducted using an aluminum rod (ρ = 2700 kg/m³) as the calibration specimen. Natural frequencies were measured in two states: without added mass (ω_1) and with a known additional mass (ω_2). The mass moment of inertia was then computed using:

$$I_o = \frac{(I_{cal} + I_{mass})(\omega_2^2 - \omega_1^2)}{\omega_1^2 - \omega_2^2}$$

where:

- I_{cal}: mass moment of inertia of the calibration rod
- I_{mass}: mass moment of inertia of the added mass
- ω_1, ω_2: angular frequencies without and with the added mass, respectively

This approach, based on standard practices, assumes linear elastic behavior and negligible damping during calibration. Incorporating the calibrated I_o into the GCTS CATS software ensures accurate measurements of shear wave velocity and shear modulus. All calibration and testing procedures were performed in accordance with ASTM D4015 guidelines for resonant column testing of soils.

At each strain level, the shear modulus (G) was computed from the updated resonant frequency, and damping ratio (D) was determined. The outcome of each test was a set of shear modulus vs. strain (G–γ) and damping ratio vs. strain (D–γ) data, typically normalized by G_{max} for analysis and comparison.

2.3 Data Processing and Interpretation

The raw output from the laboratory tests consisted of resonant frequency and damping measurements at various strain levels for each test (RC data). These were processed to compute engineering parameters. The shear modulus values from RC were normalized as G/G_{max} to facilitate comparison of modulus reduction behavior between samples. Damping ratio values were plotted versus log shear strain to examine material damping characteristics. Empirical curves were fitted to the G–γ data using a modified hyperbolic model (Darendeli, 2001), Empirical curves were fitted to the G–γ data using a modified hyperbolic model (Darendeli, 2001). The best-fit parameters, reference strain (γ_{ref}) and curvature exponent (a), were extracted for each confining pressure.

Additionally, the effect of confining pressure on G_{max} was evaluated by fitting a power-law relationship , where σ'_m is mean effective confining stress. This allowed to infer a pressure exponent for the soil stiffness, and to adjust measured moduli to a common reference stress for comparison across samples. All test results were tabulated and plotted, and key values were extracted for each soil for discussion.

3. Results

3.1 Soil Properties and Test Sample Characteristics

Table 1 summarizes the index properties of representative soil samples from each borehole, including natural moisture content, specific gravity, Atterberg limits, void ratio, and USCS classification. All tested specimens were fine-grained alluvium from the Islamabad area, generally characterized by low to intermediate plasticity and an average void ratio of ~0.8. Natural moisture contents ranged from 9–13%, while Atterberg limits indicated plasticity indices (PI) between 1 and 9, typical of low-plasticity silts (ML) and borderline silty clays (CL-ML). Two samples (BH-04 and BH-15) with slightly higher plasticity (PI = 9) were classified as lean clay (CL). Unconfined compressive strengths measured using a pocket penetrometer generally ranged from 100–200 kPa, indicating stiff consistency.

3.2 SEM and XRD

Scanning electron microscopy (SEM) images of the tested silty clay (dry, powdered form) reveal a heterogeneous microstructure composed of angular, plate-like particles with loosely packed aggregates and significant micro-porosity. At low magnification, the images highlight the aggregated structure and heterogeneity of the sample matrix. Higher magnification SEM images further reveal edge-to-face and edge-to-edge particle contacts, typical of silty clay mineral platelets (Fig. 3). Energy-dispersive X-ray spectroscopy (EDS) analysis complements the SEM observations by confirming the presence of major elements typical of silty clay mineralogy: oxygen (61%), silicon (8%), aluminum (3.5%), and iron (0.7%), alongside minor components (K, Mg, Ca) (Fig. 3). These data support the interpretation of a predominantly silicate matrix (illite/kaolinite) with minor carbonate or iron oxide phases. The lack of visible pore water films and the observed microstructural features indicate the suitability of dry testing for small-strain dynamic behavior characterization in low-PI silty clays (as per ASTM D4015).

Figure 4 shows the X-ray Diffraction (XRD) analysis conducted on the dry powdered silty clay sample. The diffraction pattern exhibits distinct peaks, with a prominent reflection at 2θ ≈ 26.75° corresponding to quartz (SiO_2) the dominant crystalline phase, comprising approximately 75% of the sample. Additional peaks in the 20°–30° range confirm the presence of clay minerals such as kaolinite and illite (13%), typical of fine-grained alluvial soils. Peaks corresponding to muscovite and biotite (11%) identify the mica

group, while minor reflections from calcite (1%) are also observed. This mineralogical composition supports the silty clay classification and the low plasticity measured in index tests. Quartz-rich, non-expansive mineralogy and observed plate-like fabrics are consistent with high small-strain stiffness and comparatively low damping. These features explain why the soils maintain stiffness at microstrain levels but show progressive modulus reduction as particle contacts are mobilized at higher strains. The limited proportion of swelling clays further reduces hysteretic damping, directly linking mineralogy to the nonlinear seismic response documented in this study (see Discussion). In particular, the dominance of quartz (~75%) provides a rigid particle skeleton, while the limited clay fraction (~13% illite/kaolinite) explains the low PI values (≤9) and moderate modulus reduction. Together with mica (~11%), this assemblage accounts for the consistently high stiffness and low damping observed in mechanical tests (next section).

The edge-to-face and edge-to-edge contacts among clay platelets observed in SEM images likely enhance stiffness at very small strains, but as strain increases these contacts are progressively mobilized, producing the nonlinear modulus reduction trends documented in this study. Similarly, the limited clay fraction and absence of expansive minerals reduce interparticle sliding hysteresis, explaining the relatively low damping ratios observed in resonant column tests.

Table 1. Representative index properties, moisture content ranges, and USCS group classification of borehole samples

Bore Hole	Specific Gravity (Gs)	Moisture Content (%)	Plastic Limit (%)	Liquid Limit (%)	PI	Void Ratio (e)	Group Name	Group Symbol
BH-01	2.67	10–13	26.73	21.98	4	0.84	Silty Clay (low plasticity)	CL-ML
BH-02	2.65	9–12	26.67	24.95	2	0.81	Silt (low plasticity)	ML
BH-03	2.68	10–14	19.82	25.56	6	0.87	Silty Clay (low plasticity)	CL-ML
BH-04	2.69	8–10	9.62	18.43	9	0.9	Lean Clay	CL
BH-05	2.67	10–13	25.39	29.4	4	0.82	Silty Clay (low plasticity)	CL-ML
BH-06	2.65	9–12	20.46	22.93	2	0.78	Silt (low plasticity)	ML
BH-07	2.65	9–12	21.18	23.78	3	0.79	Silt (low plasticity)	ML
BH-08	2.66	9–12	19.29	22.23	3	0.71	Silt (low plasticity)	ML
BH-09	2.66	9–12	17.91	21.18	3	0.71	Silt (low plasticity)	ML
BH-10	2.65	8–11	20.46	21.49	1	0.72	Silt (low plasticity)	ML
BH-11	2.66	9–12	20.28	23.53	3	0.75	Silt (low plasticity)	ML
BH-12	2.66	9–12	21.53	24.85	3	0.81	Silt (low plasticity)	ML
BH-13	2.67	9–12	18.29	21.29	3	0.81	Silt (low plasticity)	ML
BH-14	2.65	9–12	-	-	NP	0.78	Silt (low plasticity)	ML
BH-15	2.69	10–14	23.67	32.48	9	0.88	Lean Clay	CL

Gs = specific gravity of soil solids; w = moisture content; PL = plastic limit; LL = liquid limit; PI = plasticity index; NP = non plastic; e = void ratio; group name and group symbol per USCS classification

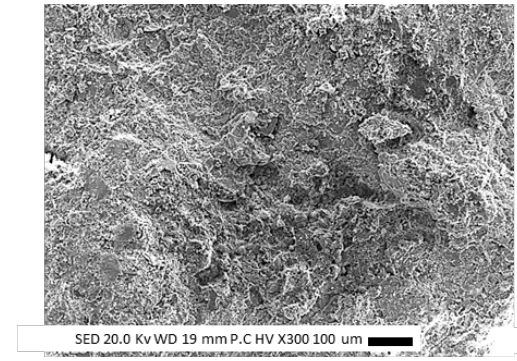

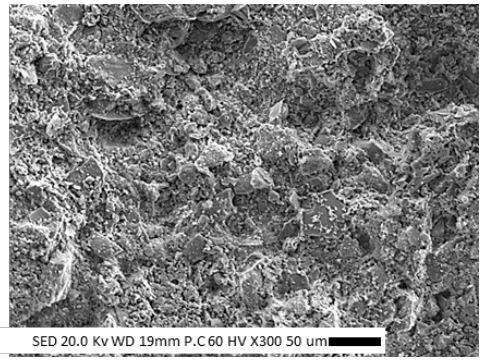

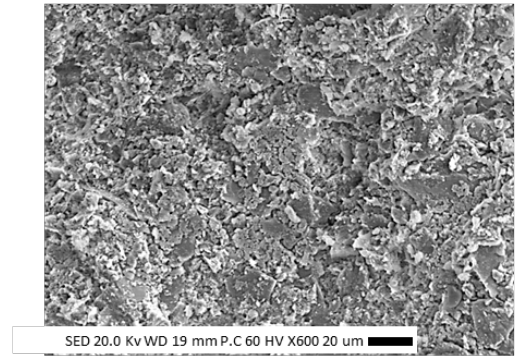

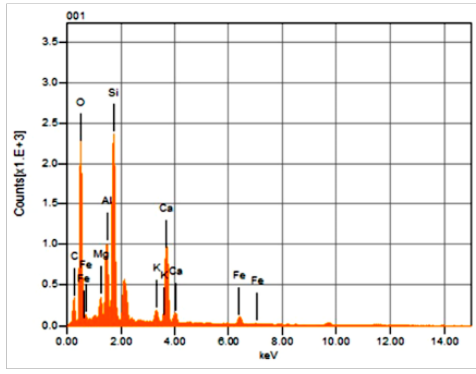

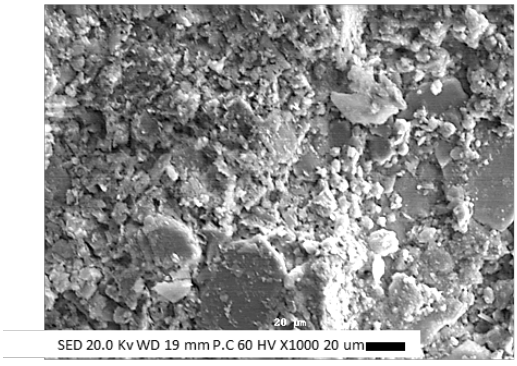

Formula	mass %	Atom %	Sigma	Net	K ratio	Line
C	13.99	20.93	0.04	8076	0.0021	K
O	54.36	61.05	0.15	61717	0.0745	K
Mg	1.62	1.20	0.04	8424	0.0040	K
Al	5.29	3.52	0.05	35016	0.0132	K
Si	12.92	8.26	0.08	88610	0.0322	K
K	1.23	0.56	0.03	7312	0.0041	K
Ca	8.48	3.80	0.06	51255	0.0300	K
Fe	2.13	0.68	0.05	5215	0.0065	K
Total	100	100				

Figure 3. SEM images show platy, angular morphology of silty clay; EDS confirms a silicate-rich matrix dominated by O, Si, Al, and Fe, characteristic of low-PI clay minerals

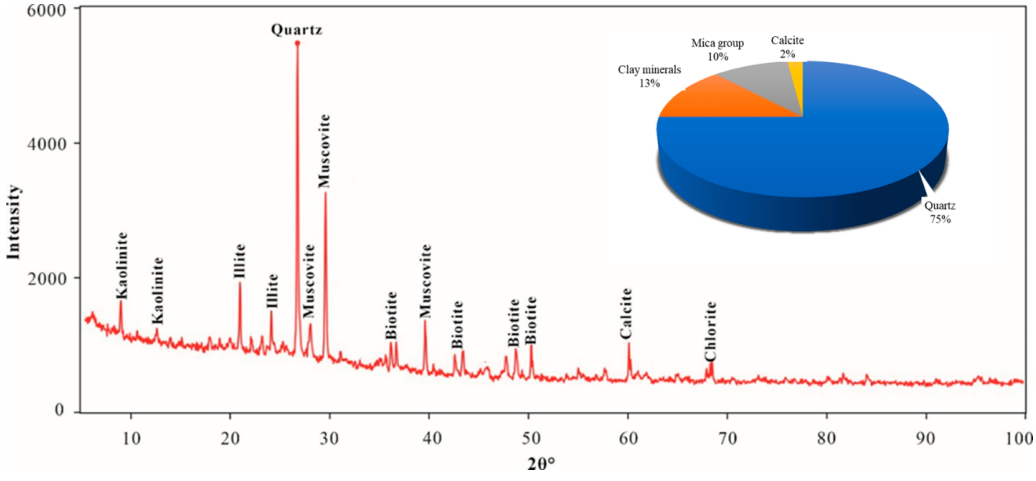

Figure 4. XRD pattern of the tested silty clay identifying dominant mineral phases

3.3 Small-Strain Shear Wave Velocity and Shear Modulus

Figures 5(a)–(c) present the comprehensive variation of shear wave velocity (V_s) with shear strain across 15 boreholes for confining pressures of 50 kPa, 100 kPa, and 150 kPa. At very small shear strains (< 0.001%), shear wave velocity values remain near their maximum, highlighting the intact, elastic soil structure. Repeatability tests on duplicate specimens from two boreholes (not shown) indicated variations of less than ±3% in Vs and G_{max} and ±5% in damping ratios across the measured strain range. This level of agreement is consistent with typical resonant column variability reported in the literature, supporting the robustness of the dataset. Across all 15 boreholes, typical small-strain V_s values range from approximately 160~180 m/s for 50 kPa, 180~250 m/s for 100 kPa, and 200–260 m/s for 150 kPa. These values reflect the small-strain stiffness of the silty clay matrix and align well with the expected range reported for similar soil types (Vucetic and Dobry, 1991; Darendeli, 2001).

As shear strain increases beyond ~0.001%, a gradual decrease in Vs is observed across all boreholes, indicating the onset of nonlinear soil behaviour and progressive softening of the soil skeleton. At strain levels of approximately 0.01%, V_s values typically decrease to 140–160 m/s, and at 0.05–0.1% strain, they further reduce to 120–150 m/s, consistent with strain-induced rearrangement and reduced inter-particle stiffness.

The effect of confining pressure is evident in the higher small-strain V_s values observed at increased confining pressures, confirming its well-known role in enhancing small-strain stiffness. At small strains, V_s values cluste tightly across all boreholes, aligning with the 150–250 m/s range reported for low-plasticity cohesive soils (L'Heureux & Long, 2017; Wang et al., 2017). As strain increases beyond ~0.001%, V_s progressively decreases converging to ~90–120 m/s by 0.1% strain, consistent with trends observed by Mog and Anbazhagan (2022) in similar silty clays. While data scatter increases slightly at strains >0.03%, it remains consistent with natural variability and experimental noise, reinforcing the robust pattern of nonlinear V_s softening across different confining pressures and borehole sites.

Fitting a power-la relationship (yielded an exponent n ≈ 0.18, lower than typical values (~0.3–0.5**) for granular soils and many clays (Hardin & Drnevich, 1972; Vucetic & Dobry, 1991; Darendeli, 2001). This reduced stress dependence aligns with the moderate plasticity possible over consolidation or aging effects of the tested silty clays, which limit the sensitivity of stiffness to confining pressure changes. Similar behavior has been reported for low-PI or lightly bonded clays, suggesting a more gradual stiffness increase with depth in these Islamabad soils compared to typical sands or highly plastic clays.

Absolute values of small-strain stiffness measured in Islamabad soils place them within NEHRP site class D (stiff soil) and approaching site class C in certain zones, aligning well with prior indirect estimates for the region, for instance, previous SPT-based approximations near the Margalla Tower site suggested V_s in the range of 175–350 m/s (Mahmood et al., 2016; Khan and Khan, 2017; Aaqib et al., 2024). The direct laboratory measurements confirm that the surficial Islamabad lays and silts are generally stiff (but not hard or cemented), comparable to other alluvial deposits in tectonically active regions (Anastasiadis et al., 2001; Govindaraju and Bhattacharya, 2012; Kanlı et al., 2006; Kockar et al., 2010) .

Shear Modulus Reduction with Strain

Figures 6(a)–(c) illustrate the variation of shear modulus (G) with shear strain for all 15 boreholes tested at investigated confining pressures. These plots collectively capture the essential strain-softening behavior of the soils and emphasize the pronounced effect of confining pressure on small-strain stiffness and modulus reduction.

At very small strain amplitudes ($\gamma < 0.0015\%$), the shear modulus remained nearly constant, with G_{max} values across all boreholes approximately: 50 kPa: 45–65 MPa, 100 kPa: 40–70 MPa, and 150 kPa: 50–80 MPa. This clear increase in $\mathbf{G}_{max}$ with confining pressure aligns with the established relationship between effective stress and small-strain stiffness (Vucetic & Dobry, 1991; Darendeli, 2001; Theland et al., 2021; Cha et al., 2014), and confirms that even in a heterogeneous site like Islamabad, confining pressure systematically enhances soil particle contacts and shear stiffness. As shear strain exceeded ~0.0015%, modulus reduction became more pronounced across all boreholes, reflecting strain-softening due to inter-particle slippage and structural rearrangement. Similarly, modulus reduction behavior did not differ noticeably between soils with PI near 9 and non-plastic silts, with all curves falling within the ±15% variability envelope.

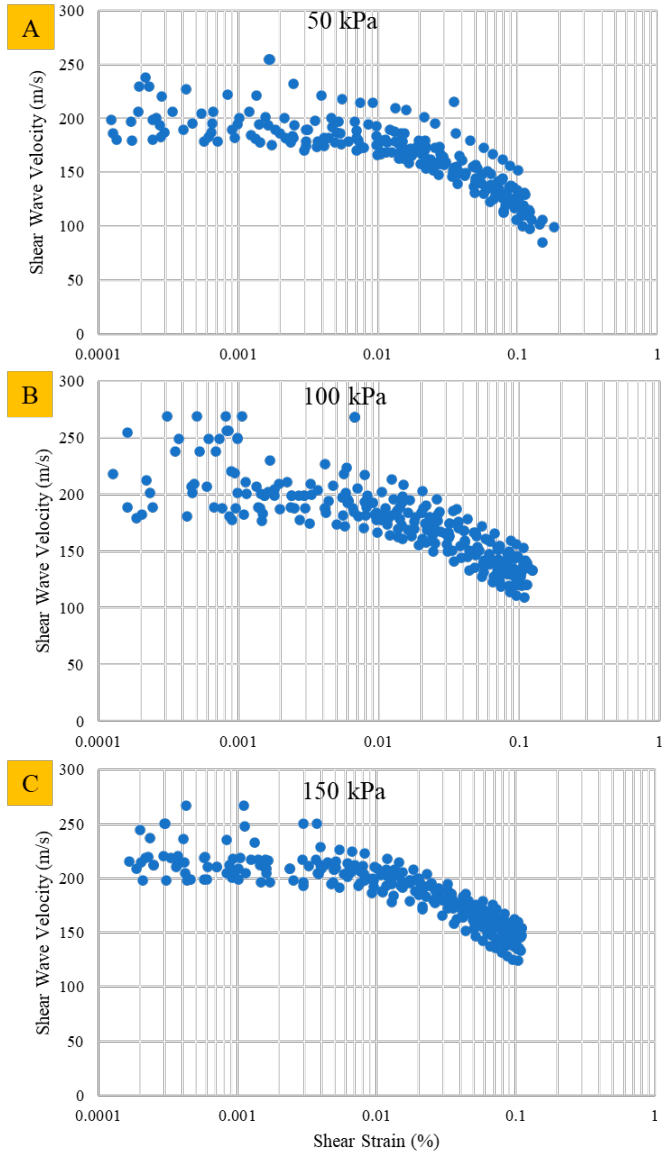

Figure 5. Shear wave velocity versus shear strain for 15 boreholes at 50 kPa, 100 kPa, and 150 kPa, illustrating confining-pressure-dependent nonlinear stiffness reduction

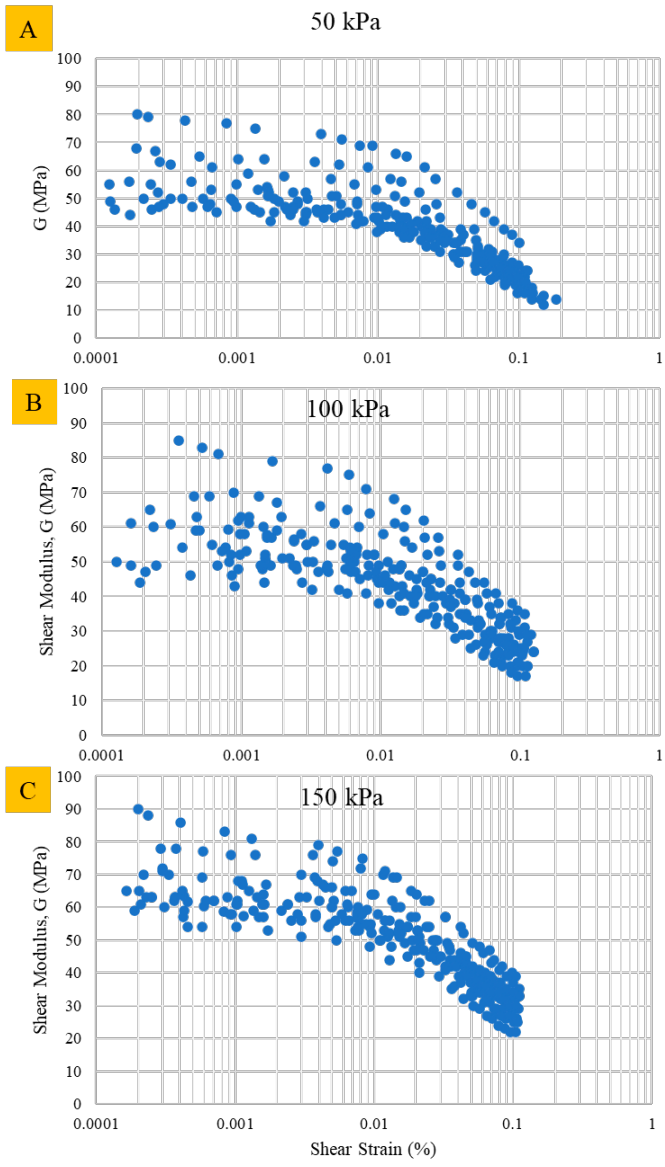

Figure 6. Shear modulus variation with shear strain across 15 boreholes at confining pressures of 50 kPa, 100 kPa, and 150 kPa

Figures 7(a)–(c) present the variation of normalized shear modulus (G/G_{max} ith shear strain for the 15 boreholes. Across all boreholes, the initial stiffness plateau (G/G_{max} ~1) was observed consistently below 0.001% strain, while as strain increased, a gradual yet clear softening trend developed. This trend was particularly evident in comparing the overall rate of modulus reduction across different confining pressures: at 0.01% strain, G/G_{max} values for the 15 boreholes clustered higher for 150 kPa (0.85–0.95) compared to 50 kPa (0.80–0.90). At 0.1% strain, G/G_{max} values for 150 kPa grouped closer to 0.5, reflecting how higher confining pressure mitigates stiffness reduction and delays the onset of significant modulus reduction trends noted by Darendeli (2001) and Vucetic and Dobry (1991). The maximum strains tested in this study were approximately 0.18% at 50 kPa, 0.12% at 100 kPa, and 0.11% at 150 kPa. At these maximum strains, the normalized shear modulus (G/G_{max}) decreased to about 0.32, 0.41, and 0.52, respectively demonstrating a consistent moderate nonlinearity. This behavior reinforces that while these silty clays retain significant stiffness at small strains, nonlinear site response analysis is essential for large earthquake strains due to appreciable softening starting at ~0.01% strain.

These consistent results across 15 boreholes reinforce confidence in the experimental data and emphasize the importance of incorporating pressure-dependent modulus reduction curves in nonlinear site response models. Minor variability at larger strains highlights the site-specific nature of soil microstructure and stress history, while the tight grouping of curves within ±15% confirms the overall reliability of the modulus reduction trends. The observed increase in small-strain moduli with confining pressure suggests higher wave propagation speeds and impedance contrasts in deeper, denser layers, which will reduce nonlinear effects during strong shaking and enhance the accuracy of seismic site response analyses and microzonation in Islamabad.

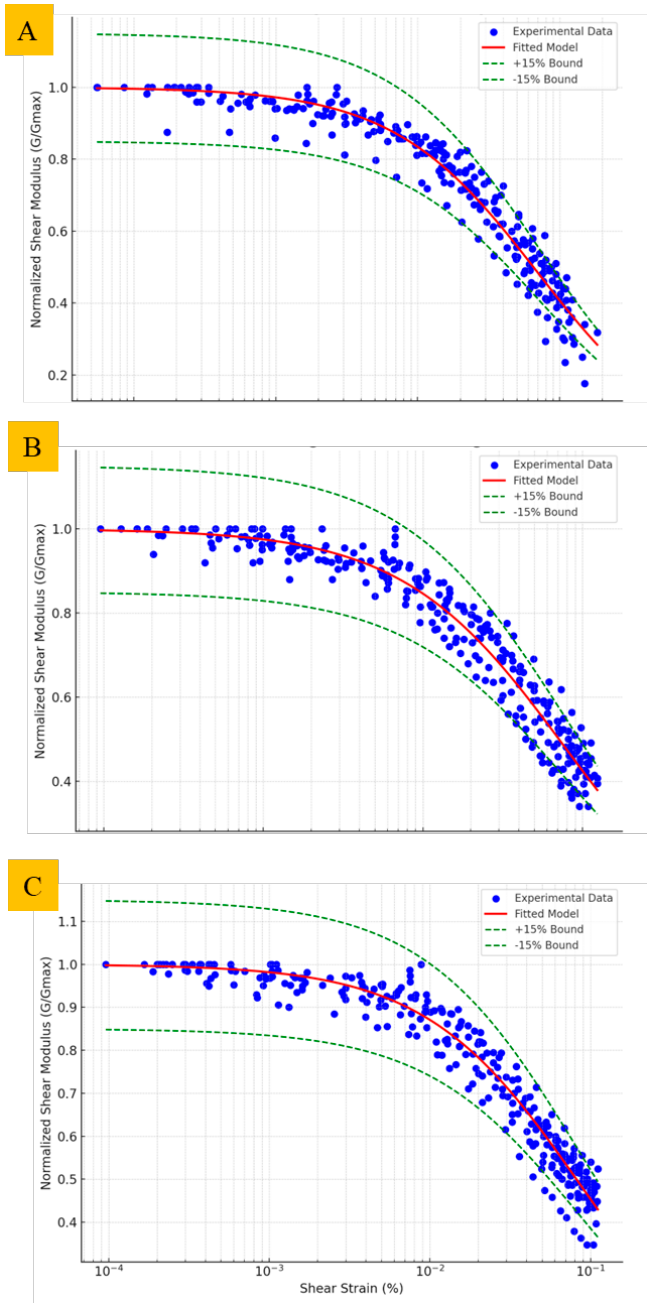

Figure 7. Normalized shear modulus (G/G_{max}) versus shear strain for soils from 15 borehole specimens at confining pressures of 50, 100, and 150 kPa. Data points represent the complete dataset, with best-fit curves and ±15% confidence bands illustrating variability across all specimens

Figure 8 compiles the normalized shear modulus (G/G_{max}) versus shear strain (γ) data from all 15 borehole samples tested at confining pressures of 50 kPa, 100 kPa, and 150 kPa. Data points are represented as blue circles (50 kPa), green squares (100 kPa), and red triangles (150 kPa), while solid lines represent best-fit curves for 50 kPa (blue) and 150 kPa (red), developed using the Darendeli (2001) modified hyperbolic model.

The Darendeli model expresses the normalized shear modulus reduction as:

$$\frac{G}{G_{max}} = \frac{1}{1 + \left(\frac{\gamma}{\gamma_{ref}}\right)^{a}}$$

where γ is the shear strain, γ_{ref} is the reference shear strain (at which $G/G_{max}=0.5$), and a is a fitting exponent that governs the curvature of the modulus reduction trend.

For each pressure condition (50 kPa and 150 kPa), best-fit values of γ_{ref} and a were determined by minimizing the sum of squared errors between measured and predicted G/G_{max} values. This approach ensures the model accurately captures both the initial stiffness plateau and the progressive softening at larger strains. The resulting fitted curves closely align with the experimental data, with deviations generally within ±15% up to ~0.05% strain, showing the reliability of the fits and the experimental trends.

At small strains (<0.001%), G/G_{max} remains close to 1.0 across all pressures, reflecting the linear elastic response of the soil matrix. As strain increases, modulus reduction initiates gradually. At 0.01% strain, G/G_{max} values typically range from 0.88–0.95 (150 kPa), 0.85–0.9 (100 kPa), and 0.80–0.88 (50 kPa). At 0.1% strain, these values reduce to 0.50–0.58 (150 kPa), 0.45–0.53 (100 kPa), and 0.38–0.48 (50 kPa). The maximum shear strains tested were approximately 0.18% (50 kPa), 0.12% (100 kPa), and 0.11% (150 kPa), with corresponding G/G_{max} values of about 0.32, 0.41, and 0.52, respectively.

The 100 kPa data consistently fall within the 50 kPa–150 kPa fitted envelope, confirming smooth transitional behaviour with confining pressure. Overall, this figure underscores the pronounced confining pressure dependence of modulus reduction in Islamabad's silty clay and clayey silt soils. The close alignment between experimental data and the Darendeli model fits highlights the robustness of the dataset and the necessity of incorporating pressure-specific G/G_{max} curves in nonlinear site response analyses for accurate seismic hazard assessment in Islamabad.

Table 2 presents the fitted γ_{ref} and exponent a values for the tested soils at 50, 100, and 150 kPa, compared against widely cited empirical models (Darendeli, Vucetic & Dobry, Vardanega & Bolton, Zhang et al.). The fitted γ_{ref} values increase systematically with confining pressure (0.065–0.082%), while the curvature exponent a remains stable (~0.87–0.91). These values fall within or slightly above published ranges for low-plasticity silts and clays, confirming the consistency and reliability of the experimental dataset.

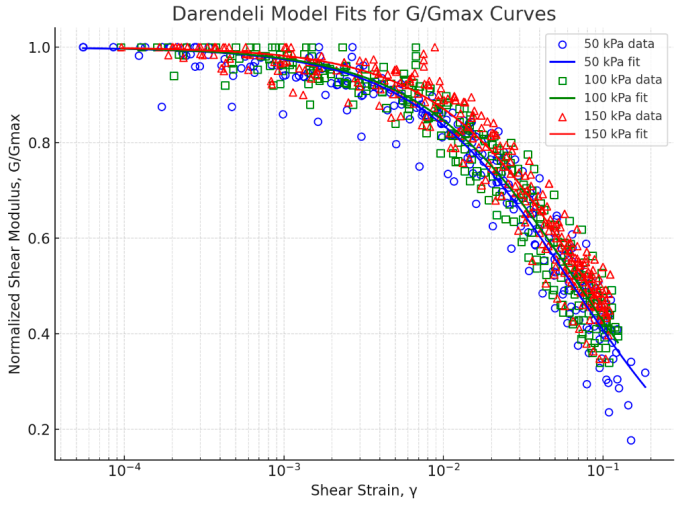

Figure 8. Normalized shear modulus (G/G_{max}) curves for soils tested at confining pressures of 50, 100, and 150 kPa. Data points represent results from all 15 borehole specimens, and best-fit curves were developed using the Darendeli (2001) modified hyperbolic model

Figure 9 illustrates the correlation between the measured normalized shear modulus (G/G_{max} and the calculated values obtained using the modified hyperbolic model across three confining pressures: 50 kPa, 100 kPa, and 150 kPa. Across all three pressure levels, the calculated G/G_{max} values exhibit a strong linear correlation with the measured data, as indicated by consistently high R^2 values of 0.95 and low RMSE values ranging from 0.045 to 0.051. The alignment of the data along the 1:1 line confirms that the adopted model captures the strain-dependent modulus reduction on with high accuracy. Notably, the spread of points slightly increases at lower normalized modulus values ($G/G_{max} < 0.5$), reflecting the inherent variability in soil behavior at larger shear strains. Nevertheless, the close clustering of data around the diagonal in all cases underscores the model's ability to reliably represent nonlinear stiffness behavior across a range of confining pressures.

Table 2. Best-fit modulus reduction parameters (modified hyperbolic model) and comparison to common models

Curve / Model	Reference strain, γ_{ref} (% strain)	Exponent, a (–)	Notes
50 kPa (fit)	0.065	0.87	This study
100 kPa (fit)	0.071	0.87	This study
150 kPa (fit)	0.082	0.91	This study
Darendeli (2001)	~0.07	~0.90	Typical for low-PI soils; PI-dependent
Vucetic & Dobry (1991)	0.04–0.08	0.8–1.0	Plasticity-dependent families
Vardanega & Bolton (2013)	0.05–0.08	~0.85	Meta-analysis (PI, confining stress trends)
Zhang et al. (2005)	0.06–0.09	~0.90	Low-to-moderate PI silts/clays

Model form $G/G_{max} = [1 + (\gamma/\gamma_{ref})^{a}]^{-1}$

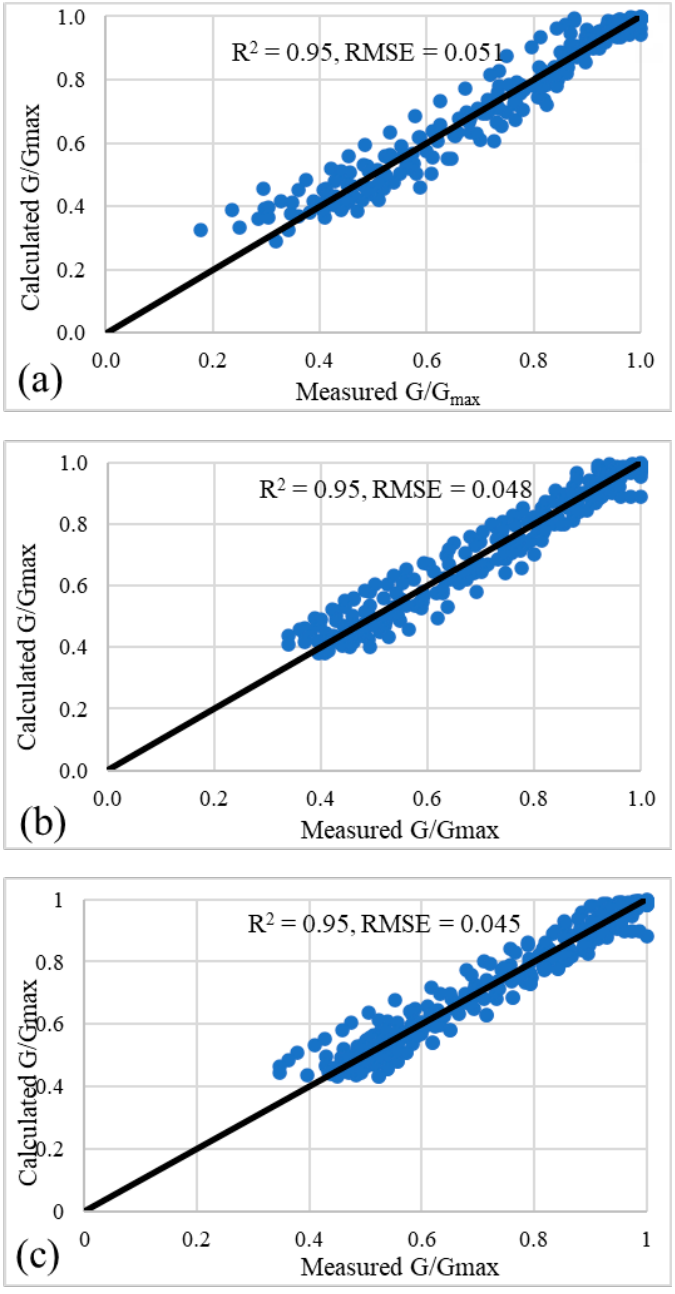

Figure 9. Comparison of measured and calculated normalized shear modulus (G/G_{max}) around the 1:1 line at confining pressures: (a) 50 kPa; (b) 100 kPa; (c) 150 kPa

3.5 Material Damping Characteristics

The material damping ratio (D) of the Islamabad silty clay soils (PI ≈ 7) was measured using both the steady-state vibration (SSV) and free vibration decay (FVD) methods in resonant column tests across a broad strain range (~0.0001%~0.1%) (Fig. 5). At very small strains ($\gamma \approx 0.001\%$), both methods yielded consistent and low damping ratios (0.5–1.5%), reflecting the quasi-elastic limit where the soil skeleton dissipates minimal energy. Across all tests, the minimum damping ratio (D_{min}) was consistently ~0.5–1% at microstrain levels, while the maximum damping ratio (D_{max}) reached ~10–12% at shear strains of 0.1%. This low small-strain damping is typical of dense, low-plasticity silty clays and implies limited attenuation of minor vibrations—an important consideration for seismic site response. As shear strain increased into the 0.001–0.01% range, damping ratios rose gradually. By $\gamma \approx 0.01\%$, damping ratios reached ~3–5%. In the 0.01–0.1% strain interval, damping increased more rapidly, reaching maximum values of ~10–12%.

At very small strains (<0.005%), the FVD and SSV damping estimates align closely, confirming the reliability of either approach in the linear viscoelastic range. However, at medium and large strain amplitudes (>0.005%), the FVD-derived damping ratios consistently increased more rapidly with strain, especially under higher confining pressures. This divergence reflects the FVD method's superior ability to capture nonlinear, strain-dependent energy dissipation, as it is not constrained by frequency response symmetry assumptions that limit the SSV approach.

To accurately model the strain-dependent damping behaviour of the soil samples across different confining pressures, the experimental damping ratio data (for both FVD and SSV) were fitted using a modified hyperbolic equation, inspired by the frameworks of Hardin and Drnevich (1972).

The equation is expressed as:

$$\lambda(\gamma) = \lambda_{min} + (\lambda_{max} - \lambda_{min}) \left(\frac{\gamma}{\gamma + \gamma_r} \right)^{a}$$

where $\lambda(\gamma)$ is the damping ratio at shear strain γ, λ_{min} and λ_{max} represent the minimum and maximum damping ratios respectively, γ_r is the reference strain capturing the transition zone, and a is a shape parameter dictating the curve's steepness. In this study, λ_{min} was fixed to the minimum observed experimental damping ratio for each confining pressure to ensure consistency with small-strain behaviour. The other parameters (λ_{max}, γ_r, and a) were determined by nonlinear least-squares fitting to the experimental data, enabling site-specific calibration.

To substantiate the use of the adopted damping ratio model in this study, it is important to highlight that several contemporary and classical works have employed or supported similarly structured equations involving reference strain and curve-shaping parameters. For instance, (Wichtmann et al., 2015) proposed empirical expressions for damping ratio as a function of shear strain, where parameters analogous to γ_r and α controlled the curvature and transition slope. Similarly, Araei and Ghodrati (2017) applied nonlinear regression to predict damping behaviour using confining pressure, strain amplitude, and frequency factors intrinsically linked to the parameters of the current model. Conti et al. (2020) also formulated constitutive models where damping evolution followed strain-sensitive transitions governed by steepness and shift parameters. These precedents validate the theoretical basis and practical applicability of the chosen model, particularly for low-plasticity soils under dry testing conditions, as in this study.

Figures 10-11 compare SSV and FVD damping ratio measurements at confining pressures of 50 kPa, 100 kPa, and 150 kPa. At 50 kPa, the data are closely grouped along the 1:1 line, with most points falling within the ±15% bands, reflecting excellent agreement between methods. The ±15% bands shown in the plots represent an engineering tolerance envelope that encompasses the scatter of measured data across all borehole samples. As confining pressure increases to 100 kPa, the scatter widens slightly, with some data points extending beyond the ±15% bands but still remaining within ±30%, indicating moderate variability. At 150 kPa, the scatter is more pronounced, and a few data points fall outside the ±30% bands. However, this variability appears to be random, rather than a systematic underestimation by the SSV method.

Overall, these results highlight the generally strong agreement between SSV and FVD methods across confining pressures, with most data within ±30% of the 1:1 line. The increased scatter at higher pressures likely reflects the nonlinear soil behavior and measurement sensitivity under these conditions, rather than a consistent measurement bias. This aligns with findings by Mog and Anbazhagan (2022) and Vucetic and Dobry (1991), who also noted that SSV and FVD methods typically agree well at small to moderate strains, while slight divergence at larger strains is expected due to measurement complexities. The data also revealed that confining pressure had a minor but consistent effect on damping behavior. At equivalent strain levels, higher confining pressures slightly reduced damping ratios likely because increased confinement constrains the soil skeleton, reducing microslip and hysteresis at inter-particle contacts. However, this effect was modest and not pronounced enough to necessitate pressure-specific damping curves for engineering analysis.

The minimum damping ratios (D_{min}) extrapolated as $\gamma \rightarrow 0$, were about 0.5–1%, slightly lower than typical published values (often 1–2%) for similar low-PI silty clays (Mog & Anbazhagan, 2022; Wang & Stokoe, 2022). From an earthquake engineering perspective, this low small-strain damping implies that small earthquake tremors or high-frequency shaking components may be less attenuated, potentially transmitting more vibrational energy to structures—a caution also highlighted by (Rahman et al., 2021). At larger strain levels during strong earthquakes, however, the observed increase in damping (up to 10–15%) would help limit extreme amplification.

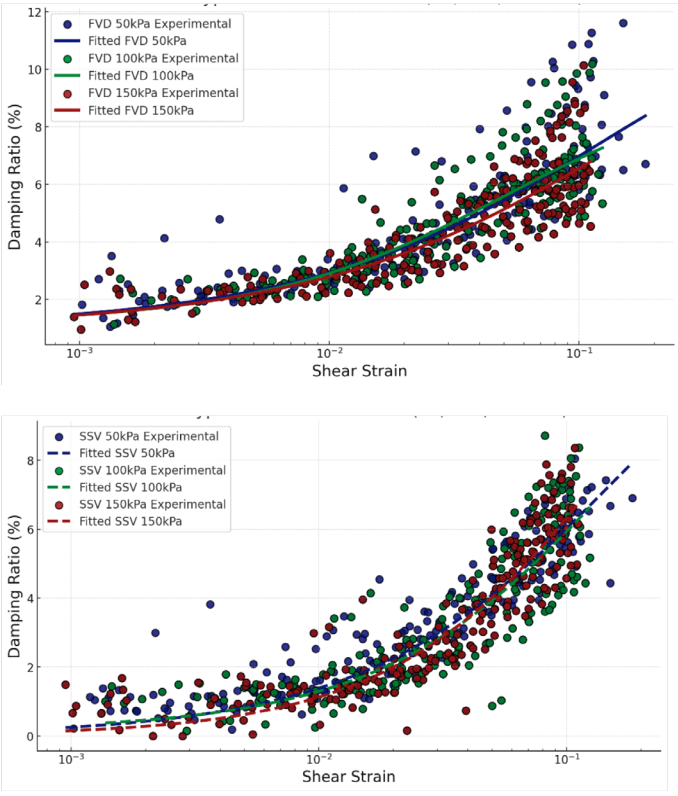

Figure 10. Damping ratio versus shear strain for FVD and SSV measurements at 50 kPa, 100 kPa, and 150 kPa, with experimental data and fitted hyperbolic curves

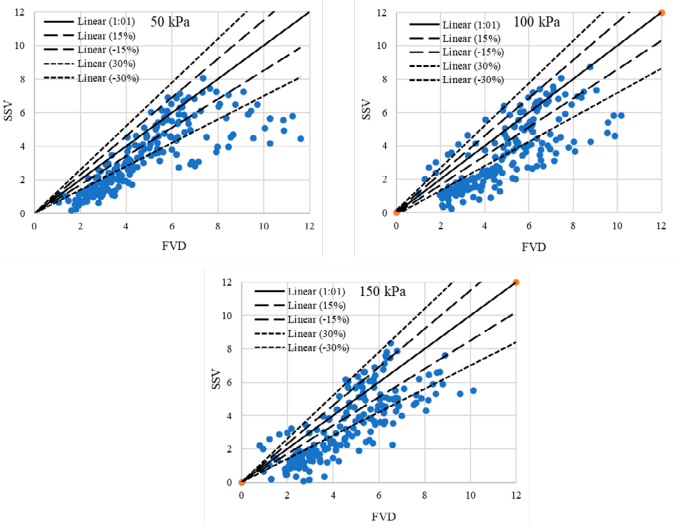

Figure 11. Comparison of damping ratios (SSV vs. FVD) with ±15% and ±30% confidence bands around the 1:1 line at confining pressures: (a) 50 kPa; (b) 100 kPa; (c) 150 kPa

Figure 12 compares the measured and calculated damping ratios obtained from the modified hyperbolic model across three confining pressures: 50 kPa, 100 kPa, and 150 kPa, for both FVD (frequency domain) and SSV (single sinusoid) methods. At 50 kPa, the SSV method yields a relatively strong correlation ($R^2 = 0.86$, RMSE = 0.76), outperforming FVD ($R^2 = 0.75$, RMSE = 1.17), which shows greater scatter and underprediction at higher damping levels. At 100 kPa, both methods demonstrate slightly reduced performance ($R^2 \approx 0.72$–0.74), with comparable RMSE values around 1.07%, suggesting similar predictive capacity but modest divergence from the 1:1 line. The best fit is observed at 150 kPa, particularly for SSV ($R^2 = 0.87$, RMSE = 0.80), indicating that damping behaviour becomes more reliably captured in stiffer soils under higher confining stress. Across all pressures, the model shows a consistent tendency to underpredict damping ratios, especially in the mid-to-high damping range. The FVD method exhibits greater dispersion, particularly at lower confining pressures, while the SSV method offers better alignment at 50 and 150 kPa. These results affirm the validity of the adopted damping model while emphasizing the influence of estimation method ad confining pressure on fitting accuracy.

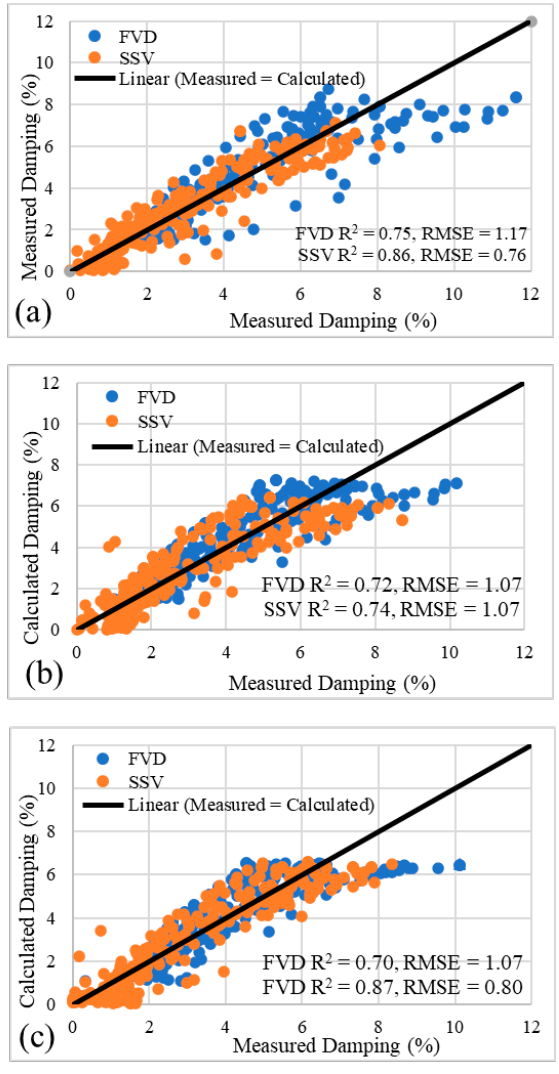

Figure 12. Comparison of measured and calculated damping around the 1:1 line at confining pressures: (a) 50 kPa; (b) 100 kPa; (c) 150 kPa

Figure 13 presents the variation of damping ratio with normalized shear modulus (G/G_{max}) for the tested silty clay at confining pressures of 50 kPa, 100 kPa, and 150 kPa. The data consistently show that damping ratio increases as G/G_{max} decreases, reflecting increased energy dissipation with progressive modulus reduction. At small shear strains ($G/G_{max} \approx 1$), the damping ratio is

low and similar across all confining pressures. As strain increases, the damping ratio rises more sharply, particularly at higher confining pressures (100 kPa and 150 kPa), indicating enhanced energy dissipation with higher confinement. These results indicate the nonlinear and pressure-dependent damping behaviour of the low-plasticity silty clay (Vucetic & Dobry, 1991).

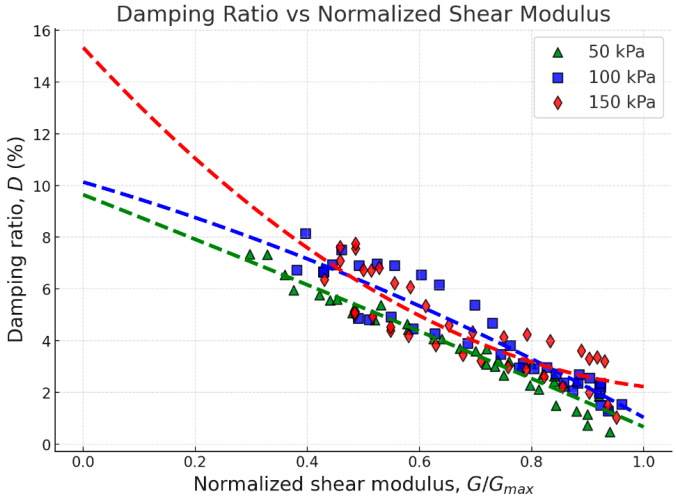

Figure 13. Variation of damping ratio with normalized shear modulus at confining pressures of 50 kPa, 100 kPa, and 150 kPa, with experimental data and fitted polynomial curves.

4. Discussion

Figure 14 compares the experimentally fitted curves for the tested silty clay soil at confining pressures of 50 kPa, 100 kPa, and 150 kPa against well-established standard models (Vucetic & Dobry, 1991; Darendeli, 2001; Zhang et al., 2005).

Figure 14a compares the measured normalized modulus reduction (G/G_{max}) curves for the tested silty clay soil at 50, 100, and 150 kPa confining pressures with established empirical models for PI=15. At small shear strains ($\gamma < 0.001\%$), all models and the tested data exhibit near-unity stiffness, confirming the elastic response of the soil matrix. As strain increases, the tested data show a more pronounced reduction in G/G_{max} compared to the predictions by Vucetic and Dobry (1991) and Vardanega and Bolton (2013), particularly at large strains ($\gamma > 0.01\%$). This observation is consistent with the findings of Guerreiro et al. (2012) and Kishida (2017), who reported that low-PI silty clays exhibit accelerated modulus reduction at larger strains and higher confining pressures.

The closer alignment of the tested data with the Darendeli (2001) and Zhang et al. (2005) models particularly at intermediate strain levels reflects the importance of confining pressure and PI on modulus reduction in low-plasticity silty clays. These comparative trends underscore that while generalized models provide valuable upper and lower bounds for engineering design, site-specific calibration remains critical for accurately capturing the nonlinear behaviour of silty clays subjected to dynamic loading.

Figure 14b presents the variation of normalized shear modulus (G/G_{max}) with shear strain (γ) for the tested silty clay at 50, 100, and 150 kPa confining pressures, overlaid with predictions from standard models. At low strains ($\gamma < 0.001\%$), the tested soil data show near-unity G/G_{max} across confining pressures, consistent with the intact elastic response described by Vucetic and Dobry (1991) and Darendeli (2001). As strain amplitude increases, the modulus reduction in the tested data aligns more closely with the Darendeli (2001) and Zhang et al. (2005) predictions, particularly for the PI=15 lower-bound trends reported in studies like Guerreiro et al. (2012) and Kishida (2017).

However, notable deviations appear at higher strains ($\gamma > 0.01\%$), where the tested data consistently degrade faster than Vucetic and Dobry (1991) and Vardanega and Bolton (2013) models predict highlighting the limitations of these models for low-PI, low OCR silty clays under higher confining pressures. This observation resonates with findings Kishida (2017), who identified that the Vucetic and Dobry (1991) model tends to overestimate stiffness at large strains for low-PI soils, unlike the Darendeli and Zhang models which better capture this nonlinear modulus reduction trend.

The separation between the standard models' upper and lower bounds (PI=100 vs. PI=15) underscores the role of plasticity in modulating strain-dependent modulus reduction. The fact that the tested data consistently fall within or below the lower bound (PI=15) trends suggests that the tested soil's low plasticity ($PI < 7$) is a key factor governing its pronounced modulus reduction. The mineralogical composition helps explain these discrepancies. The dominance of quartz (~75%) and mica (~11%) creates a rigid particle framework that increases small-strain stiffness and limits energy dissipation, while the limited clay fraction (~13% illite/kaolinite) reduces plasticity and moderates modulus degradation. In contrast, the Vucetic & Dobry (1991) and Darendeli (2001) models were developed from soils with higher clay content and plasticity, which naturally display greater softening and higher damping. This difference highlights the importance of incorporating site-specific mineralogical context when interpreting dynamic soil properties and selecting appropriate ground response models.

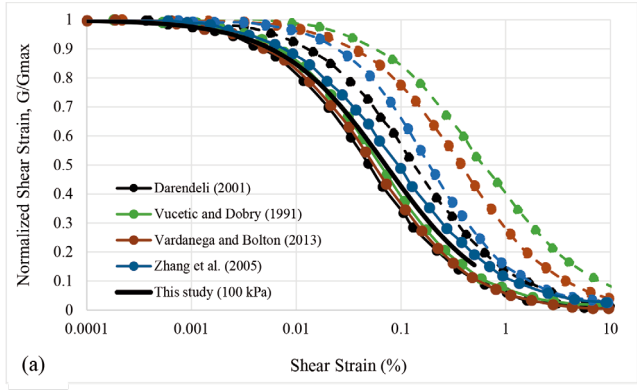

Figure 14. Comparison of normalize shear modulus (G/G_{max}) versus shear strain: (a) Fitted curve at 100 kPa confining pressure compared with standard modulus reduction models for PI = 15 and PI = 100; (b) Experimental curves at 50, 100, and 150 kPa compared with standard modulus reduction models

Figure 15 presents a comparative evaluation of the experimentally derived damping ratio curves from this study using both frequency domain (FVD) and time domain (SSV) methods against several benchmark empirical models for cohesive soils. The FVD and SSV curves demonstrate consistently lower damping across the full strain range compared to standard models, especially beyond shear strain levels of $\gamma = 0.01\%$.

The SSV curve remains below all reference models up to $\gamma \approx 0.03\%$, after which it closely parallels the slope of the (EPRI, 1993c) average curve but remains consistently lower in magnitude. The FVD curve initially aligns with the Darendeli (2001) model for PI = 15 at 100 kPa, diverging downward beyond $\gamma = 0.03\%$, and eventually falling below all empirical curves except

the EPRI and SSV lines. This trend highlights a systematic underestimation of damping for moderate to large strains ($\gamma > 0.01\%$), with the FVD and SSV curves peaking at ~8% and ~6%, respectively, at 0.2% strain, compared to >15–20% for Darendeli's high-PI models. However, the deviation remains within ±15% of the measured values, which is considered acceptable for most engineering ground response analyses. The current model therefore provides sufficiently reliable input for design purposes, though future refinements may explore pressure-sensitive adjustments to improve mid-strain accuracy.

These discrepancies are likely attributed to the soil's low plasticity index (PI < 7) and dry testing conditions, which inherently limit hysteretic damping and pore-fluid-related energy dissipation. This behaviour is in agreement with studies such as Guerreiro et al. (2012) and Mog and Anbazhagan (2022), who reported similarly subdued damping in dry, low-PI silty clays.

Furthermore, classic experimental curves by Ishihara et al. (1975), Taylor et al. (1975), and Kokusho et al. (2005) developed for higher-plasticity cohesive soils show notably higher damping (e.g., ~18–21% at 0.01–0.1% strain), emphasizing the divergence for low-PI materials. The Vucetic and Dobry (1991) model, formulated for PI ≈ 15, overlaps significantly with Darendeli's predictions and further contrasts the more restrained damping observed in this study. All curves reflect the expected nonlinear increase in damping with strain, the fitted curves from this study offer a more conservative, site-specific estimate of energy dissipation suitable for Islamabad's stiff, over consolidated silty clays. These findings underscore the critical role of PI-sensitive and site-calibrated models in ground response analysis, particularly in tectonically active regions with dominantly low-plasticity soils.

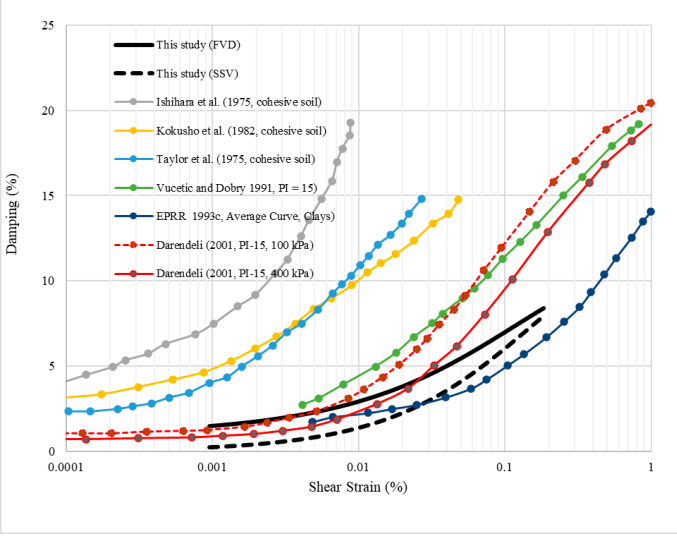

Figure 15. Comparison of fitted damping ratio curves from this study (FVD and SSV methods) with established empirical models for cohesive soils

For engineering practice, the measured curves provide more accurate, site-specific input than generic models, particularly for site class D soils prevalent in Islamabad. These curves can directly inform nonlinear site response analyses and soil-structure interaction modeling, addressing gaps in existing building codes and moving beyond reliance on proxy-based V_s estimations. Previous site response and microzonation studies in Islamabad (Khan & Khan, 2017; Adeel et al., 2023; Raza et al., 2025) have reported amplification factors of approximately 2–4× for mid-period ground motions. The laboratory-derived modulus reduction and damping characteristics presented in this study align with those findings and provide direct experimental support for the reported amplification trends. Consequently, specialized ground improvement for soft soil response may not be broadly necessary in Islamabad's fine-grained deposits.

The fitted γ_{ref} and a parameters (Table 1) confirm that Islamabad soils exhibit delayed nonlinearity compared to standard low-PI models, particularly under higher confining pressures. The extracted parameters align closely with Darendeli (2001) and Zhang et al. (2005), while diverging from Vucetic & Dobry (1991) at larger strains, reflecting the mineralogical controls of quartz-rich, low-clay matrices. This dataset already has important implications for microzonation and ground motion prediction, offering a more realistic basis for site-specific seismic demand. While these fine-grained soils appear competent and non-liquefiable, further study should evaluate potential sandy layers. Extending this testing approach to other major cities (Karachi, Lahore, Peshawar) will help develop a national database of dynamic soil properties, complemented by in-situ geophysical measurements to validate laboratory-derived curves and ensure their field relevance. Overall, the results enhance the seismic design toolkit, supporting more reliable, site-adapted hazard assessments and structural performance predictions.

5. Conclusions

This study presents the first laboratory-based evaluation of the small-strain dynamic properties of Islamabad soils using resonant column tests. Silty clay and clayey silt samples from 15 boreholes exhibited high initial stiffness, with maximum shear modulus (G_{max}) increasing systematically with confining pressure (45–80 MPa across 50–150 kPa). Normalized modulus reduction (G/G_{max}) curves showed gradual softening, with values decreasing to 0.3–0.5 at ~0.1–0.2% strain. Damping ratios ranged from ~0.5–1% at microstrains to ~10–12% at higher strains. These values were consistent across boreholes, with repeatability within ±3–5%. Best-fit γ_{ref} values increased from 0.065% at 50 kPa to 0.082% at 150 kPa, with exponent a stable at ~0.87–0.91. These parameters confirm pressure-dependent nonlinearity consistent with international reference models.

Comparison with standard empirical models (Vucetic & Dobry, 1991; Darendeli, 2001) demonstrated that Islamabad soils retain higher stiffness and lower damping than predicted for PI = 15–100 clays. The dominance of quartz (~75%) and mica (~11%) in the mineralogy explains the high stiffness and low damping, while the limited illite/kaolinite fraction (~13%) accounts for the low PI values (≤9) and moderate modulus reduction. This mineralogical fabric, characterized by edge-to-face contacts, constrains energy dissipation at small strains but permits progressive modulus degradation at larger strains. Together, these findings highlight the need for site-specific calibration of nonlinear soil behavior in the region.

Replacing generic empirical curves with the measured site-specific dataset has direct consequences for seismic hazard assessment in Islamabad. Generic models overestimate damping and stiffness, which can underestimate amplification and lead to unconservative designs. Our curves indicate amplification levels up to 20–30% higher in the 0.1–1.0 s period range, aligning with prior microzonation studies that reported ~2–4× amplification. The developed modulus reduction and damping curves can be directly integrated into one-dimensional ground response analyses and used to refine BCP-2021 site classification and design spectra, ensuring more reliable seismic design. Incorporating these curves into microzonation and seismic code development will yield more realistic design spectra, improve hazard mapping, and support performance-based earthquake engineering for Pakistan's capital region.

Acknowledgements

We are thankful to National Centre of Excellence in Geology, University of Peshawar, Pakistan for providing facilitates for carrying out this research.

Author Contributions

The authors confirm contribution to the paper as follows: study conception and design: Waqas Ahmed; Muhammad Waseem; data collection: Muhammad Zeeshan; Salman Ahmed Khattak; analysis and interpretation of results: Muhammad Waseem, Hammad Raza; draft manuscript preparation:

Waqas Ahmed, Muhammad Yasir, Ihtisham Islam. All authors reviewed the results and approved the final version of the manuscript.

Funding

This study is supported by the Higher Education Commission of Pakistan Ref No. 20-17192/NRPU/R&D/HEC/2021.

Data availability

All data are included in the manuscript.

Conflict of interest

The authors declare that they have no known competing financial interests or personal relationships that could have appeared to influence the work reported in this paper.

References

Aaqib, M., Nguyen, V.-Q., Javaid, O., Khan, A. H., Ashraf, M. A., & Bhusal, B. (2024). Evaluation of empirical SPT N-Vs correlations using 1D site response analysis for shallow bedrock sites in Islamabad, Pakistan. *Iranian Journal of Science and Technology, Transactions of Civil Engineering*, 1-17.

Adeel, M. B., Nizamani, Z. A., Aaqib, M., Khan, S., Rehman, J. U., Bhusal, B., & Park, D. (2023). Estimation of VS30 using shallow depth time-averaged shear wave velocity of Rawalpindi–Islamabad, Pakistan. *Geomatics, Natural Hazards and Risk,* 14(1), 1-21.

Anastasiadis, A., Raptakis, D., & Pitilakis, K. (2001). Thessaloniki's detailed microzoning: subsurface structure as basis for site response analysis. *Pure and Applied Geophysics,* 158(12), 2597-2633.

Araei, A. A., & Ghodrati, A. (2017). Predictive models for normalized shear modulus and damping ratio of modeled rockfill materials. *Acta Geodynamica et Geomaterialia,* 14(1), 27-41.

BCP. (2021). *Building Code of Pakistan (Seismic Provisions) – BCP-2021*. Islamabad, Pakistan: Pakistan Engineering Council.

Blaker, Ø., & DeGroot, D. J. (2020). Intact, disturbed, and reconstituted undrained shear behavior of low-plasticity natural silt. *Journal of Geotechnical and Geoenvironmental Engineering*, 146(8), 04020062.

Boore, D. M., Thompson, E. M., & Cadet, H. (2011). Regional correlations of VS 30 and velocities averaged over depths less than and greater than 30 meters. *Bulletin of the Seismological Society of America,* 101(6), 3046-3059.

Bozyigit, I., & Altun, S. (2023). Small-strain behavior and post-cyclic characteristics of low plasticity silts. *Bulletin of Earthquake Engineering,* 21(2), 791-810.

Cha, M., Santamarina, J. C., Kim, H.-S., & Cho, G.-C. (2014). Small-strain stiffness, shear-wave velocity, and soil compressibility. *Journal of Geotechnical and Geoenvironmental Engineering,* 140(10), 06014011.

Conti, R., Angelini, M., & Licata, V. (2020). Nonlinearity and strength in 1D site response analyses: a simple constitutive approach. *Bulletin of Earthquake Engineering,* 18(10), 4629-4657.

Darendeli, M. B. (2001). *Development of a new family of normalized modulus reduction and material damping curves*. The university of Texas at Austin.

EPRI. (1993c). Electric Power Research Institute (EPRI), Guidelines for determining design basis ground motions. Method and guidelines for estimating earthquake ground motion in eastern North America, 1, TR-102293.

Govindaraju, L., & Bhattacharya, S. (2012). Site-specific earthquake response study for hazard assessment in Kolkata city, India. *Natural Hazards,* 61, 943-965.

Guerreiro, P., Kontoe, S., & Taborda, D. (2012). *Comparative study of stiffness reduction and damping curves*. 15th World Conference on Earthquake Engineering,

Hardin, B. O., & Drnevich, V. P. (1972). Shear modulus and damping in soils: measurement and parameter effects (terzaghi leture). *Journal of the Soil Mechanics and Foundations Division,* 98(6), 603-624.

Ishihara, K., Tatsuoka, F., & Yasuda, S. (1975). Undrained deformation and liquefaction of sand under cyclic stresses. *Soils and Foundations,* 15(1), 29-44.

Jadoon, I. A., Hinderer, M., Kausar, A. B., Qureshi, A. A., Baig, M. S., Basharat, M., & Frisch, W. (2015). Structural interpretation and geo-hazard assessment of a locking line: 2005 Kashmir Earthquake, western Himalayas. *Environmental Earth Sciences,* 73, 7587-7602.

Kanlı, A. I., Tildy, P., Prónay, Z., Pınar, A., & Hermann, L. (2006). VS 30 mapping and soil classification for seismic site effect evaluation in Dinar region, SW Turkey. *Geophysical Journal International,* 165(1), 223-235.

Khan, S., & Khan, M. A. (2016). Mapping sediment thickness of Islamabad city using empirical relationships: Implications for seismic hazard assessment. *Journal of Earth System Science*, 125, 623-644.

Khan, S., & Khan, M. A. (2017). Seismic microzonation of Islamabad–Rawalpindi metropolitan area, Pakistan. *Pure and Applied Geophysics,* 175, 149-164.

Khan, S., Waseem, M., & Khan, M. A. (2021). A Seismic hazard map based on geology and shear-wave velocity in Rawalpindi–Islamabad, Pakistan. *Acta Geologica Sinica-English Edition,* 95(2), 659-673.

Kishida, T. (2017). Comparison and correction of modulus reduction models for clays and silts. *Journal of Geotechnical and Geoenvironmental Engineering,* 143(4), 04016110.

Kockar, M., Akgün, H., & Rathje, E. (2010). Evaluation of site conditions for the Ankara Basin of Turkey based on seismic site characterization of near-surface geologic materials. *Soil Dynamics and Earthquake Engineering,* 30(1-2), 8-20.

Kokusho, T., Aoyagi, T., & Wakunami, A. (2005). In situ soil-specific nonlinear properties back-calculated from vertical array records during 1995 Kobe Earthquake. *Journal of Geotechnical and Geoenvironmental Engineering,* 131(12), 1509-1521.

L'Heureux, J.-S., & Long, M. (2017). Relationship between shear-wave velocity and geotechnical parameters for Norwegian clays. *Journal of Geotechnical and Geoenvironmental Engineering,* 143(6), 04017013.

Mahmood, K., Farooq, K., & Memon, S. A. (2016). One dimensional equivalent linear ground response analysis—a case study of collapsed Margalla Tower in Islamabad during 2005 Muzaffarabad Earthquake. *Journal of Applied Geophysics,* 130, 110-117.

Mog, K., & Anbazhagan, P. (2022). Evaluation of the damping ratio of soils in a resonant column using different methods. *Soils and Foundations,* 62(1), 101091.

Rahman, A. u., Najam, F. A., Zaman, S., Rasheed, A., & Rana, I. A. (2021). An updated probabilistic seismic hazard assessment (PSHA) for Pakistan. *Bulletin of Earthquake Engineering,* 19, 1625-1662.

Raza, H., Ahmad, N., Aaqib, M., Jafri, T. H., & Qureshi, M. U. (2025). Seismic site amplification characteristics of Makran subduction zone using 1D non-linear ground response analysis. *Applied Sciences,* 15(4), 1775.

Seed, H. B., & Idriss, I. M. (1970). *Soil moduli and damping factors for dynamic response analysis, Report EERC 70-10*. University of California, Earthquake Engineering Research Center, Berkeley, CA.

Sheikh, I. M., Pasha, M. K., Williams, V. S., Raza, S. Q., & Khan, K. (2008). *Environmental geology of the Islamabad-Rawalpindi area, northern Pakistan*. Regional studies of the Potwar-Plateau area, Northern Pakistan. Bulletin, 2078G.

Theland, F., Lombaert, G., Francois, S., Pacoste, C., Deckner, F., & Battini, J. M. (2021). Assessment of small-strain characteristics for vibration predictions in a Swedish clay deposit. *Soil Dynamics and Earthquake Engineering,* 150, 106804.

Vardanega, P. J., & Bolton, M. D. (2013). Stiffness of clays and silts: normalizing shear modulus and shear strain. *Journal of Geotechnical and Geoenvironmental Engineering,* 139(9), 1575-1589.

Vucetic, M., & Dobry, R. (1991). Effect of soil plasticity on cyclic response. *Journal of Geotechnical Engineering,* 117(1), 89-107.

Wang, S., Luna, R., & Yang, J. (2017). Effect of plasticity on shear behavior of low-plasticity fine-grained soil. *Journal of Materials in Civil Engineering,* 29(3), 04016228.

Wang, Y., & Stokoe, K. (2022). Development of constitutive models for linear and nonlinear shear modulus and material damping ratio of uncemented soils. *Journal of Geotechnical and Geoenvironmental Engineering,* 148(3), 04021192.

Wichtmann, T., Hernández, M. N., & Triantafyllidis, T. (2015). On the influence of a non-cohesive fines content on small strain stiffness, modulus reduction and damping of quartz sand. *Soil Dynamics and Earthquake Engineering,* 69, 103-114.

Zhang, J., Andrus, R. D., & Juang, C. H. (2005). Normalized shear modulus and material damping ratio relationships. *Journal of Geotechnical and Geoenvironmental Engineering,* 131(4), 453-464.